

Amine-functionalized (Al) MIL-53/ VTEC™ mixed-matrix membranes for H₂/CO₂ mixture separations at high pressure and high temperature

Edson V. Perez, Grace J. D. Kalaw, John P. Ferraris, Kenneth J. Balkus, Jr., and Inga H. Musselman¹⁾

Department of Chemistry and Biochemistry, The University of Texas at Dallas, Richardson, TX 75080, USA

Abstract

VTEC™ PI-1388 and 20 wt% (Al) NH₂-MIL-53/VTEC™ PI-1388 mixed-matrix membranes (MMMs) with different thicknesses were tested for gas permeation of H₂ and CO₂ from 5 to 30 bar and from 35 to 300 °C. 50/50 H₂/CO₂ mixtures were also tested at 30 bar and 250 °C with stage cuts that ranged from 0.05 to 1. Gas permeation data show that the affinity of (Al) NH₂-MIL-53 for VTEC™ PI-1388 is strong enough to perform gas separations under these conditions. At 30 bar and at temperatures above 200 °C, the performance of the MMMs for H₂/CO₂ separation improved significantly with increasing temperature. Specifically, the H₂ permeability of the MMM at 300 °C increased by 70% with respect to that of VTEC™ PI-1388 (VTEC™ PI-1388: H₂ = 85 Barrer, H₂/CO₂ = 4.0; MMM: H₂ = 144 Barrer, H₂/CO₂ = 5.8). Gas mixture separations using VTEC™ PI-1388 and the MMM depended on the stage cut and reached a maximum H₂/CO₂ separation of 7.2 for VTEC™ PI-1388 and 7.5 for the MMM at a stage cut of 0.05.

¹⁾ Author to whom correspondence should be addressed. Electronic mail: imusselm@utdallas.edu.

1. INTRODUCTION

The majority of the world's energy supply currently comes from fossil fuels, including oil, coal, and natural gas, with the United States, China, and India responsible for 70% of the total world's consumption [1]. The projected demand for energy will increase by as much as 56% by 2040, where fossil fuels are expected to continue to provide much of the energy used worldwide or until new sources of energy replace them [2]. The utilization of fossil fuels ensures a long term energy supply at a low cost either as fuel for the generation of electricity in coal plants or as feedstock for the generation of hydrogen from the gasification of coal followed by the water-gas shift reaction (WGSR) in which carbon dioxide is produced along with hydrogen (Equation 1). The WGSR is an important reaction not only for the production of fuels but also for the Haber-Bosch process in the production of ammonia from hydrogen and nitrogen (Equation 2) [3, 4], which is carried out using the hydrogen produced in the WGSR.



The use of these natural resources, however, has been detrimental to the environment and has been implicated in climate change from the excessive emission of greenhouse gases (i.e., carbon dioxide) as a result of the lack of an efficient technology to separate and capture these gases. Research to address this problem has been focused on the fabrication of new inorganic and polymer-based membrane materials for the purification of hydrogen from carbon dioxide in the WGSR [5-9]. The equilibrium of the reaction (Equation 1) can be shifted to the product side by the simultaneous removal of H_2 from the mixture, which forces the reaction to generate more

H₂. A membrane capable of efficiently separating H₂ from CO₂ *in situ* at low cost is more advantageous than other separation methods (e.g., amine-based CO₂ separation) because it requires less energy to operate. The WGSR proceeds at temperatures above 200 °C in the presence of a catalyst [10, 11], and the current demands for *in situ* H₂ separation require a P_{H₂} > 7 bar with a feed pressure of up to 27 bar [12]. Therefore, testing the performance and mechanical stability of membranes under such pressure and temperature conditions is a requirement for the screening of membranes for this application.

Previous work with carbon molecular sieve (CMS) membrane reactors demonstrated that it is possible to obtain high purity H₂ from the WGSR when a membrane is used to separate H₂ *in situ* [13, 14]. Other inorganic membranes [6], like Pd [15-18], Pd-alloy [19, 20], silica [21, 22], and zeolite membranes [23], were also tested successfully, but they face challenges to be commercially viable [24]. Thermally and chemically stable polymer-based membranes and their mixed-matrix membranes (MMMs) offer low cost and highly selective membranes that can readily be scaled up for commercialization using well documented techniques (e.g., hollow fiber [25-27], spiral [28], coated porous supports [10]). It is anticipated that the performance of these membranes will increase with increasing temperatures as has been previously shown for polymer membranes at high temperatures [29]. Moreover, the testing of membranes under industrially relevant conditions of pressure, temperature, and feed composition is of vital importance since it ultimately uncovers the limitations and demonstrates the performance of the membranes under real world conditions [30]. This is even more important for MMMs because these types of membranes require strong additive/polymer interfaces to minimize incompatibility and potential mechanical failure at high pressures and high temperatures. The use of hybrid materials in MMMs that introduce organic and inorganic components, such as metal organic frameworks

(MOFs) [31-38] and metal organic polyhedra (MOPs) [39-41], is promising. These membranes typically exhibit strong additive/polymer interfaces and high loadings. Herein, we report the preparation and testing of VTEC™ PI-1388 and (Al) NH₂-MIL-53/VTEC™ MMMs at pressures up to 30 bar and at temperatures up to 300 °C with pure H₂ and CO₂ and with H₂/CO₂ mixtures at stage cuts ranging from 0.05 to 1 to minimize concentration polarization. VTEC™ PI-1388 (referred to as VTEC™ in this work) is a commercially available polyimide with a structure similar to Kapton. The (Al) NH₂-MIL-53 MOF (referred to as NH₂-MIL-53 in this work) (Figure 1) [42-45] was used as the additive due to its high thermal stability to 400 °C, stability in water, and high ideal H₂/CO₂ selectivity of 27 [46]. Previously, this MOF was also used in the fabrication of MMMs with polysulfone (PSf) [47], a polymer with low T_g (170 – 185 °C). Improved CO₂/CH₄ selectivity at 25 wt% MOF loading and pressures up to 12 bar was reported. These results suggest that (Al) NH₂-MIL-53 might be a good additive for VTEC™-based MMMs for high temperature and high pressure H₂/CO₂ separations.

2. EXPERIMENTAL

2.1 Materials

VTEC™ polyamic acid (20 wt% in *N,N*-dimethylacetamide, DMAc) was purchased from RBI Inc. and used as received. Mylar® (polyethylene terephthalate) A92 (25 μm) sheets were purchased from Active Industries. Molecular sieves type 4A were purchased from Aldrich, washed with deionized water, and activated at 400 °C for 1 d. HPLC grade DMAc (99.8%), *N,N*-dimethylformamide (DMF, 99.8%), and acetone (99.8%) were purchased from Fisher Scientific and dried over activated 4A molecular sieves. Aluminum nitrate hexahydrate Al(NO₃)₃·6H₂O, 2-aminobenzene-1,4-dicarboxylic acid (abdc), HPLC grade water,

dichloromethane, and methanol were purchased from Sigma Aldrich and used as received. For gas permeation experiments, H₂ and CO₂ (>99.99%) and their 50/50 mixtures were purchased from Airgas.

2.2 Instrumentation and methods

X-ray diffraction (XRD) patterns were acquired using a Rigaku Ultima IV diffractometer with Cu K_α (0.154 nm) X-ray radiation. XRD patterns were acquired from 3° to 45° (2θ) at 1°/min. Attenuated total reflectance-infrared (ATR-FTIR) spectra were recorded with a Nicolet 360 FTIR spectrometer at room temperature in the range of 400-4000 cm⁻¹ using a Thermo Scientific ATR attachment equipped with a diamond crystal. Thermogravimetric analyses (TGA) from 70 °C to 1000 °C were carried out using a Perkin Elmer Pyris-1 TGA with a heating rate of 10 °C/min under a N₂ atmosphere using a platinum pan. Scanning electron microscopy (SEM) images were acquired using a LEO Gemini 1500 series microscope and a Zeiss Supra-40 FEI-SEM, both operated at 10 keV. Prior to imaging membrane cross-sections, freeze-fractured membranes were mounted on carbon tape and coated with Au/Pd using a Denton Vacuum Desk II sputter coater. Measurement of glass transition (T_g) temperatures was performed using a TA-Q400 TMA thermomechanical analyzer operated in dynamic TMA mode from 10 °C to 350 °C with temperature increments of 2 °C/min and a modulation force of +/- 0.025 N at 0.50 Hz. The sample was kept in a N₂ atmosphere purged at 50 mL/min to minimize sample oxidation. T_g measurements were obtained from the second heating/cooling cycle. High pressure, high temperature gas sorption isotherms were obtained using a high pressure volumetric analyzer HPVA-100 (Micromeritics) and a custom-built high pressure, high temperature gas sorption

apparatus [29, 39]. For these experiments, 0.4 g of MOF or 1.0 g of membrane was loaded in a 5 cm³ cell. Gas sorption equilibration times varied from 10 min for the MOF to 20 min for the membranes. Before each sorption experiment at a given temperature, the materials were degassed under vacuum at 300 °C for 1 d. The obtained isotherms were corrected with blanks for each gas acquired under the same conditions. Nitrogen sorption of the MOF at 77 K was performed using a Quantachrome Autosorb-1 gas adsorption apparatus. For gas sorption experiments at 77 K, the MOF was degassed under vacuum at 300 °C for 1 d to remove residual guest molecules from the pores.

Gas permeation measurements and gas composition analyses were carried out using a custom-built high pressure, high temperature permeameter [29] equipped with a calibrated SRI-3610 gas chromatograph (GC) with a thermal conductivity detector. GC calibration curves were generated for H₂, CO₂, and their mixtures using N₂ and He as carrier gases for H₂ and CO₂, respectively, due to limitations in thermal conductivities. In order to analyze the composition of the permeate of low flux membranes, the sampling loop of the GC was kept under vacuum and connected to a manifold equipped with a pressure transducer and metering valves. With this set up, pure permeate samples at pressures between 50 and 760 Torr were introduced into the sampling loop of the GC in order to increase the response of the detector. Since the carrier gas had to be changed for each analyte, the pressure of the permeate gas in the sampling loop was kept constant between analyses to ensure the same amount of sample was introduced when the permeate was analyzed for either H₂ or CO₂. The flat membrane permeation cell (Figure S1) was designed to accommodate the membrane between two pieces of high temperature aluminum tape (433L HD rated to 316 °C, 3M™) and 3 graphite gaskets (Grafoil®, 0.5 mm thick, Lamons) compressed between the flat surfaces of two MDC SS-316 Conflat™ style flanges [29]. This

configuration leaves a distance of 0.5 mm between the membrane and the flange to increase flow across the surface of the membrane to minimize concentration polarization during gas mixture experiments. The stainless steel flange for the downstream side incorporates a 1.0 inch stainless steel porous support (1000-.1.000-.125-2-A, Mott Corporation) to support the membrane. A stream of N_2 at 1 bar and at the experiment temperature circulates in the space between the graphite gasket and the copper gasket removing leaked feed gas from the high pressure side. The use of a copper gasket is a safety feature to retain the gases in the cell should the graphite gasket fail. To remove the retentate, four 1/8" holes were drilled at the perimeter of the feed side flange above the membrane forcing the feed gas to sweep the retentate from the center to the edges of the membrane. The holes ended in a manifold on top of the flange that is connected to a pressure regulator and mass flow controllers. With this configuration, the stage cut of the membrane was controlled for the optimal separation of gas mixtures.

The stage cut (θ) (Figure 2, Equation 3) was varied from 0.05 to 1.0 (5% to 100% recovery) to determine the minimum retentate flow to maintain a constant gas mixture feed composition to maximize H_2/CO_2 selectivity and to minimize CO_2 concentration polarization at the surface of the membrane. The typical stage cut ranges from 0.01 to 1, covering most of the retentate purge rates, Q_R , for a given flow rate across the membrane, Q_P , and feed rate, Q_F . It should be noted that the optimal stage cut is determined experimentally and corresponds to the maximum recovery of the gas of interest with a particular permeate purity. A compromise between purity and recovery has to be made in order to achieve the target separation.

With these considerations, the flow rate J (moles/sec) at a given differential transmembrane pressure, Δp , was measured experimentally, and the permeability, P , or

permeance, P/L , for a component was calculated using Equation 4, where A is the exposed area of the membrane with thickness L .

$$\theta = \frac{Q_P}{Q_P + Q_R} \quad (3)$$

$$J = \frac{AP\Delta p}{L} \quad (4)$$

The determination of P was performed following the solubility-diffusivity model using the last 60% of the pressure-time curve data in the steady state region. Ideal selectivities (α_{ij}) were calculated from the ratio of the permeabilities (P , Barrers) of the gases P_i/P_j . For all pure and mixed gas permeability measurements, a minimum of 2 membranes from separately cast films were tested. The permeability of each gas through a given membrane was measured at least 4 times. The average of the last 3 values exhibited a precision better than 95%, as determined by the percent standard deviation, which reflects the error of the permeability measurement system. Measuring the reproducibility of permeability results is especially important for mixed-matrix membranes owing to the unavoidable imperfect dispersion of the additive in the polymer matrix and can provide insight into the robustness of the membrane preparation and testing methodology. In a typical experiment, a 5.0 cm² membrane piece (Figure S2) was mounted in a stainless steel cell that exposed one side of the membrane to a pressurized feed of 5, 15, or 30 bar and the other side to an evacuated line. The entire system was evacuated for at least 6 h at the experimental temperatures of 35, 100, 200, 250, and 300 °C before a leak rate test was performed for 0.5 h for each downstream volume (70 cm³ and 350 cm³). Permeability experiments with single gases at 35 °C lasted for 2 h for thin (<20 μm) VTECTM membranes and for up to 20 h for the thicker (84 μm) MMMs due to the low CO₂ flux. At higher temperatures, the experiments lasted for 1 h for the VTECTM membranes and 2 h for the MMMs. At 35 °C, degassing times between H₂ runs lasted for 2 h for the VTECTM and MMMs

and up to 5 h for CO₂ with the MMMs. At higher temperatures, the degassing times between runs were reduced to 2 h. This protocol was repeated for each pressure increment. Permeability experiments with a 50/50 H₂/CO₂ mixture at 15 and 30 bar and at 250 °C followed the same protocol, but the duration of the experiment was increased up to 4 h with a downstream evacuation after 1 h to ensure the permeate composition corresponded to the steady state since the partial pressure of each gas in the mixture was reduced to half of the total pressure.

2.3 Synthesis of NH₂-MIL-53 crystals

Crystals of NH₂-MIL-53 were synthesized by modifying reported procedures [44, 48, 49]. In a 1000 mL round bottom flask, 15 g (83 mmol) of aminoterephthalic acid and 29 g (77 mmol) of aluminum nitrate nonahydrate were dissolved in 600 mL of deionized (DI) water. The solution was then refluxed for 15 h, cooled to room temperature, centrifuged, and the supernatant decanted. Then, 600 mL of DI water was added to the yellow paste and refluxed for 6 h, cooled to room temperature, stirred for 15 h, centrifuged, and the supernatant decanted. The yellow paste was then washed with 200 mL of DMF, centrifuged, and the supernatant decanted. The material was then refluxed for 5 h in 500 mL of DMF in a 1000 mL round bottom flask, cooled to room temperature, stirred for 15 h, centrifuged, and the supernatant decanted. The pale yellow/white paste was then washed with acetone (2 x 200 mL), filtered, and dried in a vacuum oven at 80 °C for 1 d, at 150 °C for 1 d, at 300 °C for 1 d, cooled to room temperature in the vacuum oven, and stored in a desiccator under nitrogen. A pale yellow powder (3.9 g) was recovered.

2.4 Fabrication of mixed-matrix membranes (MMMs)

For the separation of H₂ from CO₂ at WGSR conditions, polymer membranes with high thermal stability, high flux, and high selectivity are required. VTECTM is thermally stable to 500 °C [50, 51] and has a good H₂/CO₂ separation of 5.4 up to 300 °C and 3.0 MPa [29]. These properties suggest that VTECTM membranes may be promising for H₂/CO₂ separations under WGSR conditions, provided that they retain or improve their separation properties. In a previous work that tested NH₂-MIL-53/PSf MMMs for CO₂/CH₄ separations [47], it was found that MMMs with NH₂-MIL-53 loadings above 25 wt% suffered from defects that reduced their separation performance. Considering PSf has a lower T_g (170-185 °C) than VTECTM (T_g = 275 °C), it is predicted that, with the more rigid VTECTM chains, the amount of NH₂-MIL-53 that can be loaded before defects form would be 25 wt% or less. Therefore, for this study, MMMs with 20 wt% NH₂-MIL-53 loadings were prepared to avoid the potential formation of interfacial defects. Flat membranes of VTECTM were prepared by diluting the VTECTM polyamic acid dope to 12 wt% with DMAc and stirring at room temperature for 15 h. The 20 wt% NH₂-MIL-53/VTECTM MMMs were prepared by dispersing the NH₂-MIL-53 crystals in DMAc (5.4 wt% solids in DMAc) with stirring for 1 h, bath sonicating for 3 h, stirring for 1 h, and bath sonicating for 1 h. Then, the 12 wt% VTECTM/DMAc dope was added to prepare a 20 wt% NH₂-MIL-53/VTECTM mixture that was bath sonicated for 1 h and stirred for 1 d at room temperature. The solutions (VTECTM and MMM) were cast onto a Mylar[®] sheet at room temperature using an

automatic film applicator (Sheen 1133N) with a calibrated doctor blade. The membranes, still on the supported Mylar[®] sheet, were transferred to a nitrogen-purged chamber to dry for 5 h at 80 °C. Since high temperatures and long periods of time are required to induce imidization of the polyamic acid, the membranes were removed from the Mylar[®] sheet and dried on a glass substrate in a custom-built high temperature programmable vacuum oven at 80 °C for 1 d, at 150 °C for 1 d, at 300 °C for 1 d, cooled to room temperature, and stored in a desiccator purged with N₂. The resulting membranes had thicknesses ranging from 10.2 to 20.0 μm for VTEC[™] and from 48.8 to 84.6 μm for the MMMs. This variation in thickness was intentionally introduced to ensure the permeabilities of the membranes were independent of leaks or defects that might result at high pressures and high temperatures.

3. RESULTS AND DISCUSSION

3.1 NH₂-MIL-53 crystals

SEM images show that the as-synthesized crystals do not have a well-defined morphology (Figure 3a), whereas the activated NH₂-MIL-53 crystals are more rod-like with a length of <1.0 μm and a width of <200 nm (Figure 3b). This morphology was obtained after activating the as-synthesized crystals by refluxing in DMF and drying at 300 °C for 1 d.

NH₂-MIL-53 crystals were reported to conform to different space groups (monoclinic or orthorhombic) depending on the absence or presence of guest molecules in the pores of the MOF due to the flexibility of the framework [48]. This property leads to three possible conformations that can be distinguished from XRD data (Figure 4a-c): the large, narrow, and closed pore forms. The large pore form is obtained when solvent (DMF) remains in the pores (Figure 4a), whereas the narrow pore form with a pore aperture of 0.6 x 1.7 nm [42, 52] (Figure 4b) is obtained when

water remains in the pores. Complete removal of guest molecules (DMF and water) yields the closed pore form of the MOF (Figure 4c), [42, 43, 52]. In this work, the activation (refluxing in DMF and drying in vacuum at 300 °C) of the NH₂-MIL-53 crystals yielded the narrow pore form as verified by XRD (Figure 4d). Although the closed pore form is desired for H₂ separations, the pore aperture and space group of the MOF in the membrane may be set by interactions of the framework with the polymer, by the casting solvent, and by the drying conditions during the fabrication of the MMM that prevent the MOF from existing in the closed pore form, as previously described for MIL-53/Matrimid[®] MMMs [53]. Therefore, obtaining the MOF in its closed pore form before the preparation of the MMMs does not necessarily result in the retention of this conformation in the MMM. The results of these interactions can be observed in the XRD pattern of the 20 wt% NH₂-MIL-53/VTEC[™] MMM (Figure 4f) where an intense peak at $2\theta = 15.6^\circ$ replaced the main peak of the NH₂-MIL-53 crystals at $2\theta = 13.3^\circ$ (Figure 4d). Since VTEC[™] is not soluble after imidization at temperatures above 250 °C, a 20 wt% NH₂-MIL-53/PSf MMM was prepared from CHCl₃ and dried at 150 °C in order to reproduce the changes in the XRD pattern of the MOF in the MMM and to ensure that the polyamic acid form of VTEC[™] did not degrade the MOF during the fabrication process. The results show that both MMMs (from VTEC[™] and PSf) have the same XRD pattern (Figure 4f,g), suggesting that the change in XRD patterns between the MOF (Figure 4b) and the MMMs (Figure 4f,g) may arise from MOF/polymer interactions, as was previously described by Rodenas, et al. [35]. This observation is further supported by the XRD pattern of the MOF (Figure 4h) recovered after dissolving the PSf MMM in CHCl₃ and drying the MOF at 300 °C in vacuum. The XRD pattern of the recovered MOF was identical to that of the starting material, the MOF in the narrow pore form (Figure 4b). To further test the chemical stability of the MOF, the material was dispersed

in concentrated acetic acid by stirring and bath sonication followed by drying at 300 °C in vacuum. The XRD pattern of the MOF after this process (Figure 4i) was identical to that of the starting material (Figure 4b), indicating the MOF is stable in VTEC™ polyamic acid. The XRD pattern of NH₂-MIL-53 after exposure to high pressure (up to 70 bar) and high temperature (up to 300 °C) gas adsorption experiments was also obtained (Figure 4e) to verify the stability of the MOF under these conditions, which resemble the testing conditions of the MMMs. The obtained XRD pattern of this material was also identical to the XRD pattern of the starting material, confirming that the narrow pore form of NH₂-MIL-53 is highly stable.

ATR-FTIR spectra of NH₂-MIL-53/VTEC™ MMMs, shown in Figure 5a-d, indicate the MOF and the pendant amino group in the linker are stable to 300 °C and that the amine functionality is preserved before (70 and 150 °C, Figure 5c,d) and after (300 °C, Figure 5b) the imidization of the polyamic acid of VTEC™. The bands at 3400 cm⁻¹ and 3500 cm⁻¹ correspond to the NH₂ stretching mode of the NH₂-MIL-53 linker [54] and are present only in the spectra of the MMMs and pure NH₂-MIL-53 MOF. Another important band, located at 450 cm⁻¹ and corresponding to the O-Al vibration [55, 56], is also present in the MMM and the MOF spectra.

TGA of the activated NH₂-MIL-53 (Figure S3a) shows the material loses 12 wt% at temperatures up to 140 °C that can be attributed to the evacuation of water from the pores since the MOF is in the narrow pore form. Above this temperature, NH₂-MIL-53 is stable to 400 °C without further change in weight. The remaining white powder at temperatures from 600 to 1000 °C could be attributed to the formation of aluminum oxide.

The nitrogen sorption isotherm for NH₂-MIL-53 crystals at 77 K (Figure S4) shows the material exhibits the gate opening effect at P/P₀ = 0.16, which results in a continuous N₂ uptake up to P/P₀ = 1.0. The isotherm exhibits hysteresis upon desorption, which could be an indication

of N₂ condensation in the pores. Although the MOF is in the narrow pore form, and potentially in the closed pore form after degassing at 300 °C for the sorption experiments, the walls of the MOF allow the diffusion of N₂ (kinetic diameter = 0.364 nm) into the pores to a maximum capacity of 13 mmol/g. A similar isotherm with equivalent N₂ sorption capacity was achieved after multiple sorption/desorption cycles when the MOF was activated at 130 °C for 3 h, implying that guest molecules were removed from the pores of the MOF only after multiple cycles [44]. For the NH₂-MIL-53 used in this work, the high degassing temperature removed the guest molecules from the pores of the MOF more efficiently, which resulted in a high N₂ sorption capacity.

High pressure and high temperature H₂ and CO₂ sorption isotherms (Figure 6a) show that NH₂-MIL-53 has a limited sorption capacity of 2.7 mmol/g for CO₂ at 35 °C and 40 bar when compared to other materials like activated carbon that has a CO₂ sorption capacity of 8 mmol/g under identical conditions. The CO₂ isotherms at 35 °C and 100 °C show a rapid saturation of the pores at pressures <10 bar, presumably due to the affinity of the amines for CO₂. At 200 °C and 300 °C, the CO₂ sorption capacity at 40 bar is further reduced to 1 mmol/g and 0.5 mmol/g, respectively, with the isotherms showing a transition from rapid gas uptake to a slower uptake. No significant H₂ sorption in NH₂-MIL-53 was observed from the isotherms in the range of 35 °C to 300 °C and at pressures up to 70 bar, as seen in Figure 6a.

3.2 NH₂-MIL-53/ VTECTM mixed-matrix membranes (MMMs)

Optical images of imidized VTECTM and 20 wt% NH₂-MIL-53/VTECTM membranes dried at 300 °C in vacuum for 1 d (Figure 7a,d) show that the membranes have a uniform yellow/orange color, are flexible, and can be cast into large area films free of gross defects.

SEM images of the membrane cross-sections show a smooth and defect-free morphology for the VTEC™ membrane (Figure 7b,c), whereas the MMM exhibits a larger topography also free of large defects (Figure 7e,f). The MMM's cross-section also shows no significant particle aggregation and no gross MOF/polymer interfacial defects, even at high magnifications, suggesting good affinity of the polymer for the MOF. The morphologies shown in Figures 7e,f have also been observed for other MOF/polymer MMMs (e.g., MOF-5/Matrimid® 5218 [31], MIL-53/Matrimid® 5218 [53], ZIF-8/PBI [57], ZIF-8/Matrimid® 5218 [58]) and have been attributed to plastic deformation of the polymer matrix during the freeze fracture process that results from the strong interaction of the polymer with the MOF [31]. In the case of 20 wt% NH₂-MIL-53/VTEC™ MMMs, the plastic deformation is not as prominent as it is for MOF-5/Matrimid® 5218 MMMs, suggesting a softer MOF/polymer interaction. Figure 7f also shows that the morphology and size of the NH₂-MIL-53 crystals embedded in the polymer are similar to the MOF crystals shown in Figure 3b, supporting the conclusion based on XRD (Figure 4) that the NH₂-MIL-53 crystals in the MMM are not degraded during the membrane manufacturing process.

ATR-FTIR spectra of VTEC™ (Figure 5e-g) and the 20 wt% NH₂-MIL-53/ VTEC™ MMMs (Figure 5b-d) indicate that the membranes are stable to 300 °C. The degree of imidization of the polyamic acid during the drying of the membranes at different temperatures is related to changes in the 1725 cm⁻¹ band that is characteristic of the C=O vibration of the imide [59]. Visual inspection of the ATR-FTIR spectra of the VTEC™ membrane and the MMMs show 1725 cm⁻¹ to 1542 cm⁻¹ (amide, C-NH) and 1725 cm⁻¹ to 1662 cm⁻¹ (CONH) band ratios increasing with increasing temperature, indicating that imidization of the polyamic acid is achieved.

Thermogravimetric analyses of VTECTM and the MMM shown in Figure S3b,c indicate that the membranes are stable up to 500 °C, and no loss of mass is observed in this range. It can also be concluded that, up to this temperature, no residual solvent is released from the membranes, which indicates that the drying protocol (vide supra) is effective. Above 500 °C, the membranes start to decompose rapidly, leaving a carbon film at the end of the thermal cycle at 1000 °C.

High pressure and high temperature CO₂ adsorption in VTECTM membranes from 35 °C to 300 °C and up to 50 bar (Figure 6b) show a decrease in sorption capacity with increasing temperature. The isotherms at temperatures below 200 °C follow the dual mode Henry-Langmuir sorption model that describes gas sorption in glassy polymers [60], whereas at higher temperatures close to the T_g of the polymer, the isotherms exhibit a reduced Langmuir sorption capacity due to the reduction of microvoids in the polymer [61-64]. Comparing the CO₂ sorption capacities of VTECTM at 35 °C and 100 °C to other polyimides, like Matrimid[®] 5218, it can be seen that the CO₂ isotherms of Matrimid[®] 5218 at 35 °C and 70 °C [39] have almost twice the sorption capacities of VTECTM (Figure 6b). This difference in CO₂ sorption capacities may explain the highest ideal H₂/CO₂ selectivity of VTECTM of 5.3 over Matrimid[®] 5218's H₂/CO₂ selectivity of 2.7 [31]. Hydrogen sorption in the MOF, VTECTM, and MMMs was not detectable in the range of temperatures used in this work (Figure 6). Since the total gas sorption capacity in MMMs results from the contributions of the additive and the polymer [65], the isotherms of the MMMs should reflect both components if the pores of the MOF are free of solvent molecules and accessible to gas molecules. In the case of the 20 wt% NH₂-MIL-53/VTECTM MMM, the CO₂ sorption isotherms exhibit shapes that combine the shapes of the MOF and VTECTM isotherms (Figure 6c). By calculating the CO₂ sorption contribution of the neat MOF and of the

polymer in the MMM from their respective isotherms at 35 °C and 40 bar (Figure 6a,b), it can be seen that the 20 wt% MOF present in the MMM contributes with 0.6 mmol of adsorbed CO₂ and the polymer contributes with 1.2 mmol of adsorbed CO₂ adding to a total of 1.8 mmol of adsorbed CO₂ in the MMM, which is similar to the value in the CO₂ isotherm of the MMM (1.9 mmol) also measured at 35 °C and 40 bar (Figure 6c). These results confirm that the pores of the MOF in the MMM are accessible to gas molecules and that the pressure required to access the pores is <10 bar. From Figure 6a, it can be seen that the amount (2.5 mmol) of CO₂ adsorbed in the narrow pore form of the NH₂-MIL-53 at 35 °C and 30 bar is about 37% of that adsorbed in the open pore form (6.7 mmol/g) [66]. The difference in magnitude can be attributed to differences in pore volume between the two forms, where the narrow pore form may exhibit smaller pore volume than the open pore form [42].

Thermomechanical analysis of the membranes obtained from the second temperature cycle (Figure 8) show that both VTECTM and the 20 wt% NH₂-MIL-53/VTECTM MMM have a T_g between 270 °C (storage modulus and dimension change, Figure 8a,b) and 292 °C (tan δ, Figure 8c). The invariability of the T_g of the MMMs in the presence of the MOF, and the limited plastic deformation at the additive/polymer interface, shown in Figure 7e,f, suggest that, at 20 wt% loading, the amount of MOF in the MMM is not enough to significantly increase the T_g of the polymer. In addition, no crosslinking of the polymer by the MOF through the amine moiety in the linker takes place since the IR band corresponding to the amine is still present for the MMM (Figure 5a,b).

3.3 Gas permeation

3.3.1 Single gas

Pure H₂ and CO₂ permeability and H₂/CO₂ ideal gas selectivities of VTECTM and 20 wt% NH₂-MIL-53/VTECTM membranes at 5, 15, and 30 bar and from 35 °C to 300 °C, shown in Figure 9, correspond to the averages of 2 membranes for each system, the polymer and the MMM. The thicknesses of the tested membranes were 10.2 μm and 12.6 μm for VTECTM and 48.8 μm and 84.6 μm for the MMMs. The small variation in H₂ and CO₂ permeability and H₂/CO₂ selectivity between VTECTM membranes or between MMMs with different thicknesses (Figure 9 and Tables 1, T1, and T2) indicate that the measured permeability is free from interference from leaks or defects that may arise from high pressure and high temperature. Since dewetting of the MOF particles and the formation of small, isolated defects are potential problems for MMMs at high pressures and high temperatures, the testing of membranes with different thicknesses helps to determine whether the membranes are undergoing mechanical changes during the permeation experiments. If membranes of different thicknesses show similar permeabilities, then it can be concluded that the membranes are free from defects and that the MOF/polymer interface is strong enough to prevent dewetting of the MOF. The testing of MMMs under these conditions is important since MMMs require strong additive/polymer interfaces to remain mechanically stable and to retain their separation properties. The permeability data for each VTECTM membrane (Table T1) and for each 20 wt% NH₂-MIL-53/VTECTM membrane (Table T2) tested show that, regardless of the membrane thickness, the gas separation properties remain similar within each type of membrane, with little variation from membrane to membrane at temperatures up to 250 °C. At temperatures higher than the T_g of the polymer (T_g = 275 °C), the MMMs tend to exhibit larger variations in gas permeation but not in H₂/CO₂ selectivity (Table T2), indicating the potential formation of defects at the MOF/polymer interface. At 300 °C, the MMM with the largest thickness (84.6 μm) exhibited a 62% higher H₂

permeability ($H_2 = 177$ Barrer at $300\text{ }^\circ\text{C}$ and 30 bar) than the membrane with the smaller thickness ($48.8\text{ }\mu\text{m}$) ($H_2 = 109$ Barrer at $300\text{ }^\circ\text{C}$ and 30 bar), signaling the potential formation of defects. Figure 9c,d also shows that the membranes (VTECTM and MMM) exhibit a non-linear increase in H_2 and CO_2 permeability with increasing temperature that is mostly independent of the pressure even at temperatures above the T_g of the polymer. Remarkably, the observed permeabilities of H_2 and CO_2 at 5 , 15 , and 30 bar at a given temperature have little variation between measurements (Figure 9, Table 1). Ideal selectivities, however, exhibit a small increase with increasing pressure probably due to compaction of the membranes (Figure 9a,b). Higher pressures induce a tighter packing of the polymer chains, making the membrane more selective to H_2 . A comparison of the H_2 permeability at 30 bar and $300\text{ }^\circ\text{C}$ for the MMM to that of the pure polymer is shown in Table 1. The permeability for the MMM (144 Barrer) is 70% larger than the permeability for the polymer (85 Barrer), indicating that the presence of the MOF in the MMM improves the polymer's performance. The increased H_2 permeability of the MMM suggests that the NH_2 -MIL-53 may be diluting the polymer and also increasing the diffusivity of the gases in the membrane by incorporating uniform diffusional channels since the pores of the MOF are accessible to gas molecules according to the results obtained from gas adsorption (Figure 6a,c). A similar improvement for the ideal selectivities of the MMMs versus the polymer is evident in Figure 9a,b. The data show that the MMM suffers a small decrease in H_2/CO_2 ideal selectivity at 30 bar from 7.0 ($35\text{ }^\circ\text{C}$) to 5.8 ($300\text{ }^\circ\text{C}$), but remains above Knudsen selectivity (4.7). The ideal H_2/CO_2 selectivity for the pure polymer decreases from 6.0 ($35\text{ }^\circ\text{C}$) to 4.0 ($300\text{ }^\circ\text{C}$), making the MMM 45% more selective at $300\text{ }^\circ\text{C}$ than the pure polymer. The results suggest that the MOF imparts mechanical stability to the MMM at temperatures above the polymer's T_g by restricting chain mobility. The performance of the membranes under the

conditions of pressure and temperature used in this work suggest that the VTEC™ membranes and corresponding MMMs have the potential to perform gas separations at high pressure and high temperature due to the affinity of the polymer for the MOF as well as to the thermal and chemical stability of the materials used in the preparation of the MMMs.

3.3.2 Gas mixture

Although pure gas permeation data help to understand the separation properties of membranes as well as their limitations, the separation of gas mixtures under industrially relevant conditions presents a more realistic scenario to uncover the potential challenges (e.g., membrane plasticization, concentration polarization, poisoning of sorption sites by impurities in the feed, chemical stability, etc.) that MMMs may need to overcome to be commercially viable. VTEC™ (20.0 μm) and 20 wt% NH₂-MIL-53/ VTEC™ (50.6 μm) membranes were tested at 250 °C and 30 bar with 50/50 H₂/CO₂ mixtures to mimic real world conditions in order to reveal the improved properties and potential weaknesses of the MMMs for applications that may require high pressure and high temperature conditions, such as the water-gas shift reaction. The data in Table 2 show that the selectivity of the VTEC™ and the 20 wt% NH₂-MIL-53/VTEC™ membranes to the 50:50 H₂/CO₂ mixture (Figure 10) with a stage cut of 1 differ mainly due to the strong CO₂ concentration polarization on the surface of the VTEC™ membrane. This resulted in a decrease in the H₂/CO₂ selectivity to 2.9 from an ideal selectivity of 8.1. In contrast, the MMM suffered less CO₂ concentration polarization and retained a H₂/CO₂ selectivity of 4.4, albeit lower than the ideal selectivity of 8.3 observed under the same conditions (Table 1). Concentration polarization is an unavoidable consequence of the separation of two species from a mixture that can be minimized by the removal of the retentate.

To remove the retentate, the feed is supplied at the surface of the membrane at a controlled rate to force the retentate out of the cell thereby exposing the membrane to a constant feed composition. To facilitate the removal of the retentate, the original test cell was modified [29] to force the feed to sweep the retentate out of the cell by reducing the volume between the membrane and the flange. This configuration proved to be effective in recovering the selectivity of the membranes, but at the expense of reduced recovery. In the case of the VTEC™ membrane and the MMM, when the stage cut was systematically reduced from 1 to 0.05 to reduce concentration polarization, the H₂/CO₂ selectivity of the membranes increased nonlinearly until reaching a maximum at $\theta = 0.05$, where the selectivities (VTEC™ = 7.2, MMM = 7.5, Table 2) were close to their respective ideal selectivities (VTEC™ = 8.1, MMM = 8.3, Table 1). The results confirm that the VTEC™ membrane and the MMM were stable to high pressure and high temperature conditions. Our results also show that relatively low permeable membranes may not be immune to concentration polarization effects when tested for gas mixture separations and that selectivity values may need to include stage cut values for their evaluation.

To compare the performance of the MMM tested in this work, the selectivity and permeability data of VTEC™ and the MMM were plotted in a log-log plot (Figure 11). The results show that at 35 °C the performance of VTEC™ and the MMM lies below the Robeson's upper bound [67] (not shown). Figure 11 also shows that the performance of the membranes improves when tested at temperatures higher than 35 °C with pure gases and gas mixtures, as is shown by the increase in both permeability and selectivity. The improved performance of VTEC™ and the MMM with the increasing testing temperature is consistent with a model that predicts the upper bound for H₂/CO₂ separations at high temperatures [68, 69]. Interestingly, the MMM outperformed the polymer with increased ideal and gas mixture H₂/CO₂ selectivity at all

temperatures even those above the T_g of the polymer. These results show that the VTECTM and NH₂-MIL-53/VTECTM membranes have the potential to be used in high temperature and high pressure H₂/CO₂ separations (e.g., WGSR) since they exhibit improved selectivity as well as mechanical stability at pressures up to 30 bar and at temperatures up to 300 °C [12].

Since no other MOF-based MMMs have been tested at conditions similar to the high pressures and high temperatures used in this work [36, 37], we have compared our NH₂-MIL-53/VTECTM MMM results with those of other polymer membranes for the H₂/CO₂ separation. PBI, one of the most studied polymers, has a H₂/CO₂ mixture separation that ranges from 20 at 200 °C to 3 at 300 °C. Unfortunately, this polymer has low H₂ permeability (11 Barrer at 300 °C), which limits its industrial application [70]. Other high T_g polymers include Matrimid[®] and 6FDA derivatives, but they exhibit low H₂/CO₂ selectivities between 1 and 4 that are also not appealing for industrial applications [71]. Their MMMs also do not exhibit improved H₂/CO₂ separations and have not been tested with H₂/CO₂ mixtures at the conditions used in this work [71]. Compared to pure 6FDA polymers, diamine cross-linked 6FDAs also have improved H₂/CO₂ separations, but at temperatures less than 150 °C due to the instability of the amide bond. At temperatures greater than 150 °C, the selectivity reverts to that of the non-cross-linked polymer [72, 73]. For example, upon cross-linking, the H₂/CO₂ mixture separation for 6FDA-durene membranes and ZIF-71/6FDA-durene MMMs both increased at 35 °C, from 0.1 (6FDA-durene, H₂ = 86 Barrer) to 22 (6FDA-durene cross-linked with tris-(2-aminoethyl)amine or TAEA, H₂ = 287 Barrer) and to 51 (10 wt% ZIF-71/6FDA-durene cross-linked with TAEA, H₂ = 267 Barrer) [74]. However, due to the low thermal stability of the amide bond formed during cross-linking, the MMM could not be tested at higher temperatures.

A comparison of the H₂/CO₂ separation properties of the MMMs in this work with the properties of inorganic membranes under similar conditions shows that the MMMs compete favorably with some of the inorganic counterparts, with some exceptions. In a recent review that compares MOF membranes with molecular sieve membranes [75], H₂/CO₂ separations performed with several zeolite membranes showed that these membranes have not yet achieved the required robustness for industrial applications. Owing to the difficulty in preparing defect-free zeolite membranes on porous supports, chemical vapor deposition (CVD) and catalytic cracking deposition (CCD) of silanes have been used to plug large intercrystalline defects and to reduce the pore size to increase selectivity. MFI membranes subjected to post-synthesis CCD exhibited improved H₂/CO₂ separation properties at 450 °C and 1.5 bar from 5 to 19 and, in some cases, up to 100 at the expense of reducing gas permeance by an order of magnitude. The limitations for the industrial application of zeolite membranes subjected to CVD or CCD, however, are the expensive equipment, the difficulty in scaling up the fabrication process, and the pore densification that makes uncertain the long term stability of the membranes [75]. Other zeolite membranes, like ZSM-5, were also tested at temperatures of up to 400 °C and 3.9 bar with dry and wet H₂/CO₂ mixtures but showed low H₂/CO₂ selectivities of 3.5 [75]. In another study, sulfur-doped sodalite membranes showed thermal stability to 300 °C and ideal H₂/CO₂ selectivities of 5.9. Despite the small pore size (0.29 nm) [76], the membranes did not increase significantly their separation properties when compared to VTEC™ or PBI membranes. Silica membranes also exhibited good H₂/CO₂ separation factors when doped with 17-33% Nb or Pd/Co, achieving separation factors from 10 to 1500 [77], but the poor hydrothermal stability of the silica membranes is still a limitation for their large scale application. MOF membranes also show a wide range of H₂/CO₂ selectivities, from 6.5 to 13.6 for ZIF-7 (200 °C), 3.3 to 15.5 for

ZIF-8 (25 °C), 7.3 to 20 for ZIF-90 (200 °C), and 25 for ZIF-95 (325 °C) [77, 78], but these membranes are still under development and face the same challenges as zeolite membranes for their implementation in industrial gas separations. Therefore, it can be seen that MOF-based MMMs present an alternative to inorganic or MOF membranes for industrial gas separations since, according to the results presented in this work, the MOF/polymer interface could be strong enough to retain the mechanical properties of the polymer and to prevent the formation of defects in the membrane at high pressures and high temperatures.

4. CONCLUSIONS

By testing membranes of different thicknesses with pure gases and gas mixtures, this work demonstrates the applicability of MMMs for gas separations at pressures up to 30 bar and at temperatures up to 300 °C. Thermomechanical analysis and gas separation data provided evidence of the mechanical stability of the MOF/polymer interface under these conditions. By observing identical T_g values for the polymer and the MMM, and by measuring similar permeabilities and selectivities between the membranes of different thicknesses, it was demonstrated that the gas separation properties of the membranes are free of interference from leaks or defects that could have arisen during permeation experiments at high pressure and high temperature. The data also show that a stable MOF/polymer interface existed for the separation of gas mixtures at high pressure and high temperature with an improved performance. These properties, complemented with gas adsorption data of the MMMs, suggest that the MOF increases gas diffusion in the membranes at the loading of 20 wt% and that the polymer is the continuous phase that performs most of the separation. It can then be concluded that to

overcome the polymer's gas separation properties, a higher MOF loading may be required that would shift the separation properties of the MMM from the polymer's to the MOF's. This work also shows that the membrane stage cut may have a large impact on the separation properties of relatively low permeable membranes to gas mixtures, an experimental parameter that may need to be addressed in future gas mixture separations.

ACKNOWLEDGMENTS

This material is based upon work supported by the Department of Energy under Awards number DE-FE0001293 and DE-NT0007636. *Disclaimer:* This report was prepared as an account of work sponsored by an agency of the United States Government. Neither the United States Government nor any agency thereof, nor any of their employees, makes any warranty, express or implied, or assumes any legal liability or responsibility for the accuracy, completeness, or usefulness of any information, apparatus, product, or process disclosed, or represents that its use would not infringe privately owned rights. Reference herein to any specific commercial product, process, or service by trade name, trademark, manufacturer, or otherwise does not necessarily constitute or imply its endorsement, recommendation, or favoring by the United States Government or any agency thereof. The views and opinions of authors expressed herein do not necessarily state or reflect those of the United States Government or any agency thereof.

This material is based upon work supported by the National Science Foundation under Grants No. CBET-0933563 and CBET-1403950.

Appendix A. Supplementary Information

Supplementary information associated with this article can be found in the online version at [supplementary information link].

FIGURES AND TABLES

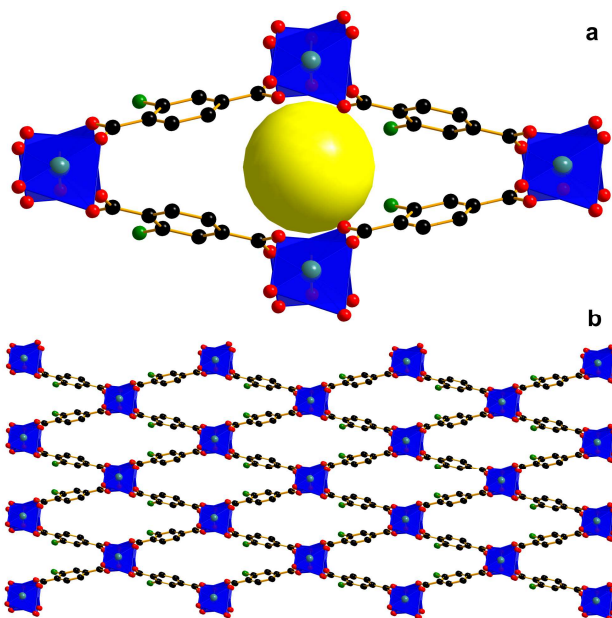


Figure 1. Structure of NH₂-MIL-53 in the narrow pore form calculated using Diamond 4 [45] and the crystallographic data in [42]: a) unit cell viewed in the *c* direction showing the available volume in the pore (yellow sphere) and b) supercell showing the 0.6 x 1.7 nm channels in the *c* direction.

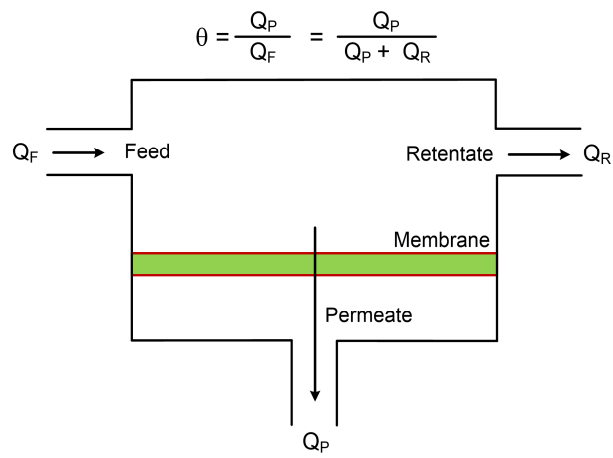


Figure 2. Representation of stage cut (θ) to reduce concentration polarization: Q_R = retentate purge rate, Q_P = flow rate across the membrane, Q_F = feed rate = $Q_P + Q_R$.

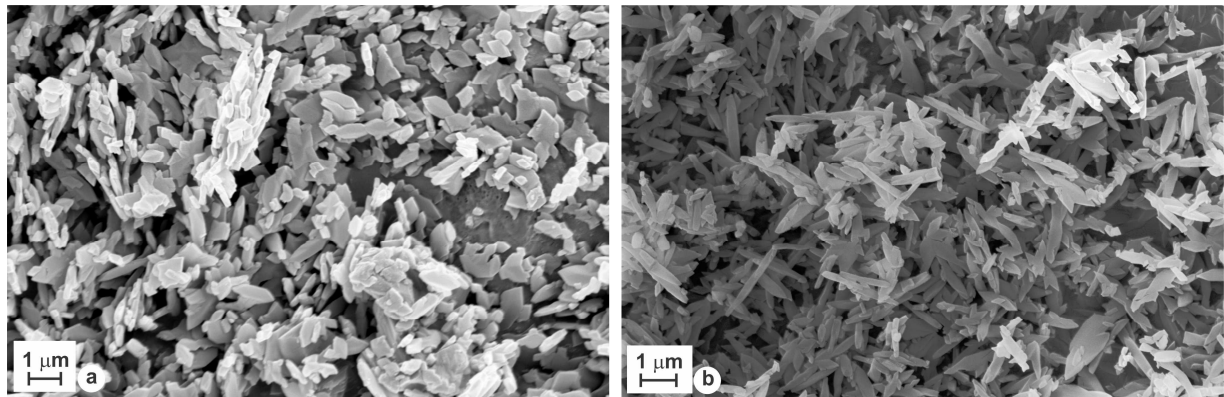


Figure 3. SEM images of NH₂-MIL-53 crystals: as-synthesized (a) and activated (b).

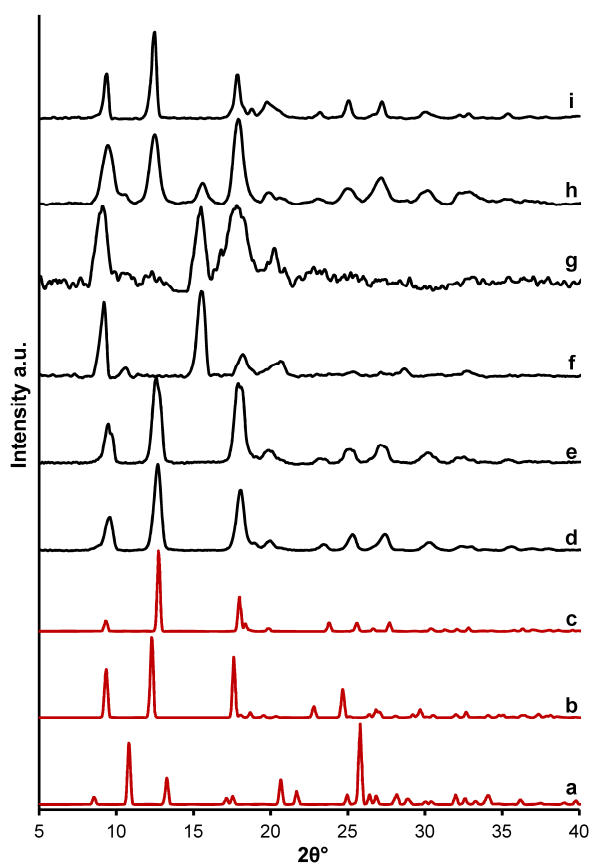


Figure 4. $\text{NH}_2\text{-MIL-53}$ theoretical (red) XRD patterns calculated using Diamond 4 [45] and the crystallographic data in [42, 52]: a) large pore, b) narrow pore, c) closed pore; $\text{NH}_2\text{-MIL-53}$ experimental (black) XRD patterns: d) $\text{NH}_2\text{-MIL-53}$, e) $\text{NH}_2\text{-MIL-53}$ after HPVA, f) 20 wt% $\text{NH}_2\text{-MIL-53/VTEC}^{\text{TM}}$ MMM, g) 20 wt% $\text{NH}_2\text{-MIL-53/polysulfone}$, h) $\text{NH}_2\text{-MIL-53}$ recovered from 20 wt% $\text{NH}_2\text{-MIL-53/polysulfone}$ MMM, i) $\text{NH}_2\text{-MIL-53}$ after dispersion in acetic acid and drying at 300 °C.

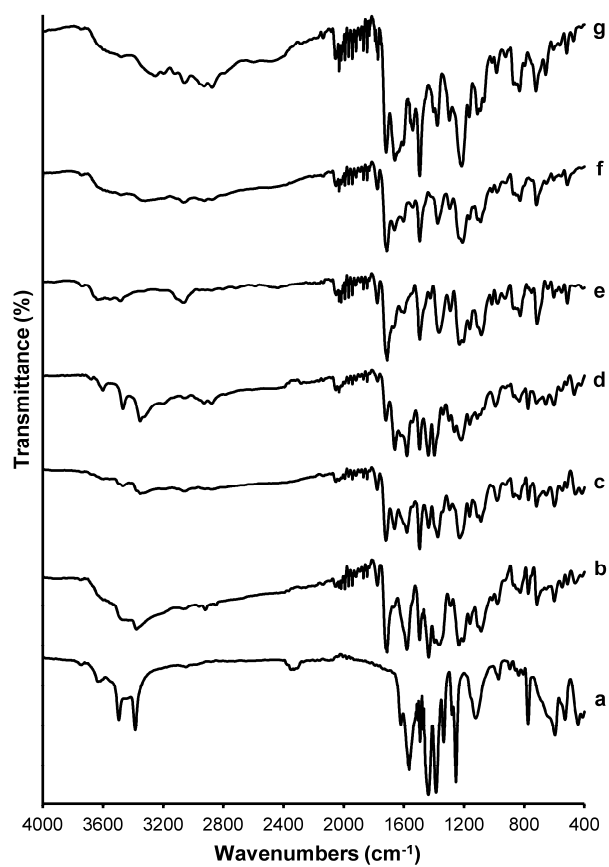


Figure 5. ATR-FTIR spectra of activated narrow pore NH₂-MIL-53 (a), 20 wt% NH₂-MIL-53/VTECTM MMM at 300 °C (b), 150 °C (c), 70 °C (d), and VTECTM at 300 °C (e), 150 °C (f), and 70 °C (g).

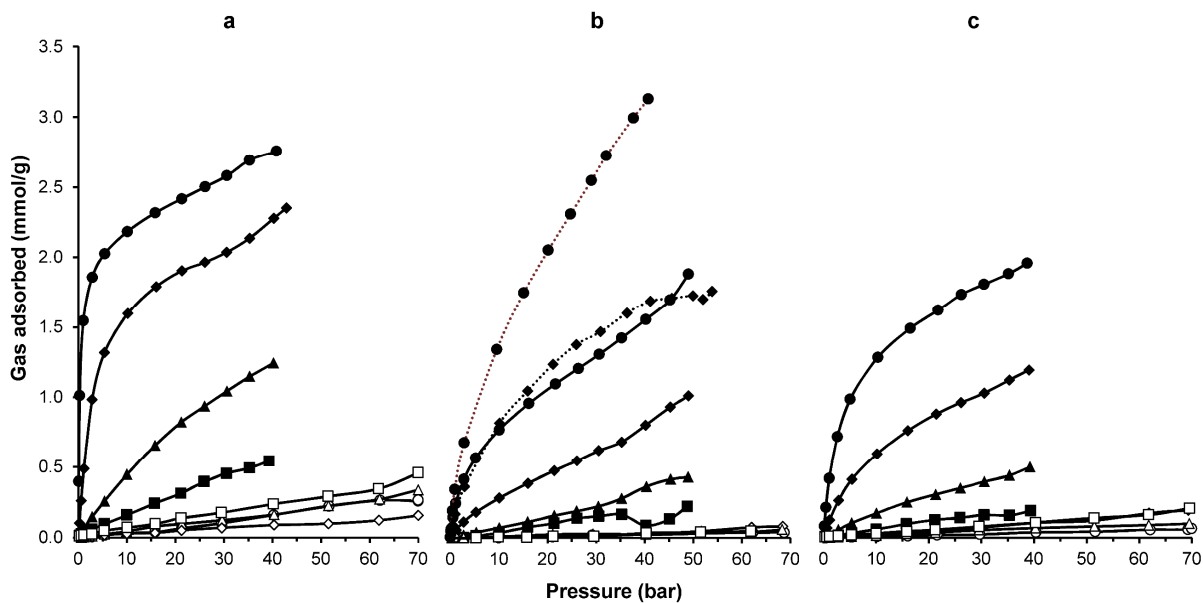


Figure 6. Gas sorption isotherms of CO₂ (solid symbols) and H₂ (open symbols) at high pressure and high temperature in NH₂-MIL-53 (a), VTECTM (b), and 20 wt% NH₂-MIL-53/VTECTM MMMs (c). (●, ○) = 35 °C, (◆, ◇) = 100 °C, (▲, Δ) = 200 °C, (■, □) = 300 °C). CO₂ sorption isotherms in Matrimid[®] 5218 (dotted lines) at 35 °C (●) and 70 °C (◆) [39] are shown for comparison in (b).

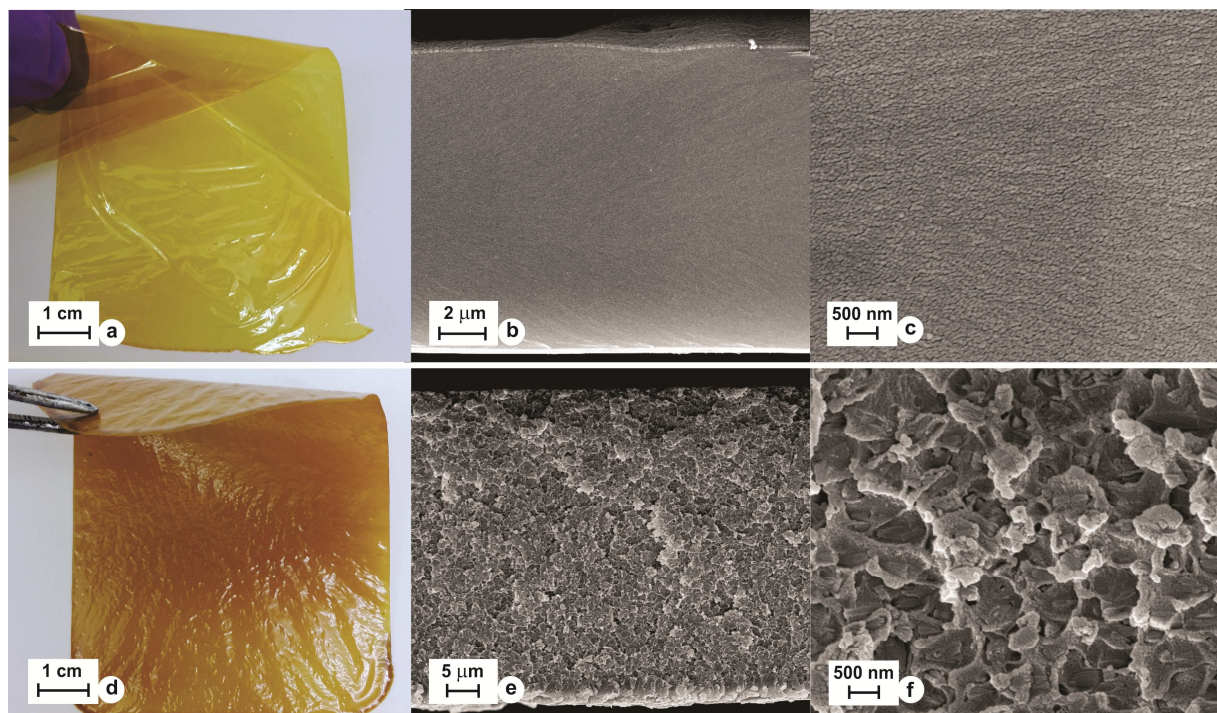


Figure 7. Optical and SEM images of a VTEC™ membrane and a 20 wt% NH₂-MIL-53/VTEC™ MMM. VTEC™: a) optical image, b) and c) cross-sections at low and high magnification, respectively. 20 wt% NH₂-MIL-53/VTEC™ MMM: d) optical image, e) and f) cross-sections at low and high magnification, respectively.

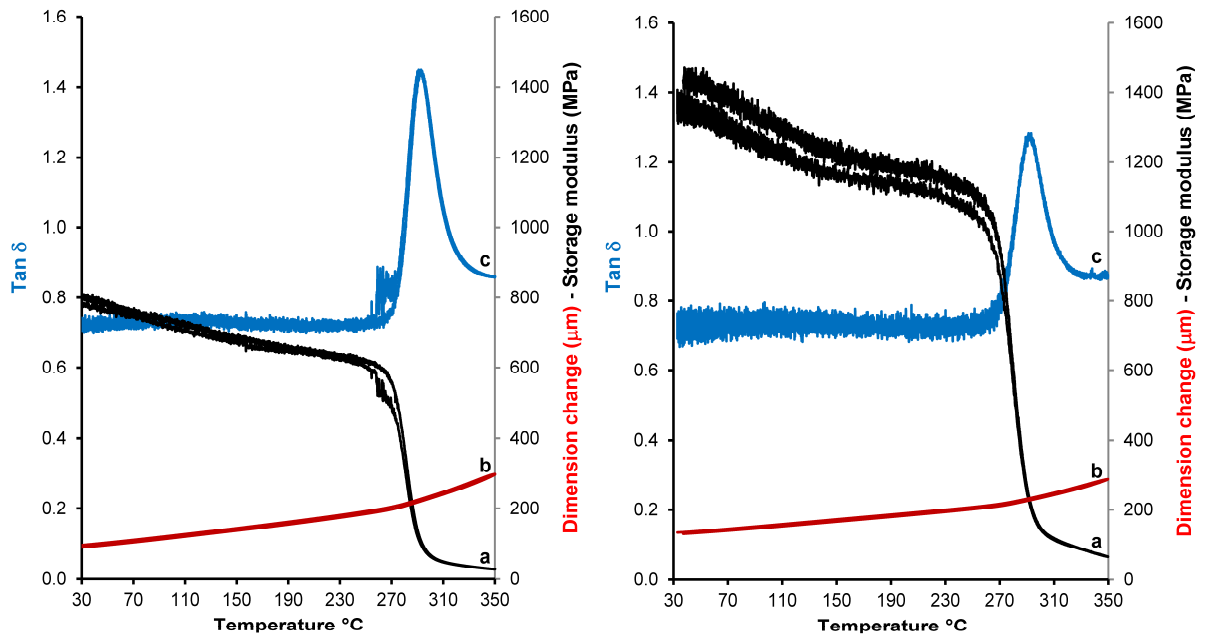


Figure 8. Dynamic TMA of VTEC™ (left) and a 20 wt% NH₂-MIL-53/VTEC™ MMM (right) showing storage modulus (a), dimension change (b), and tan δ (c) variations with temperature increments.

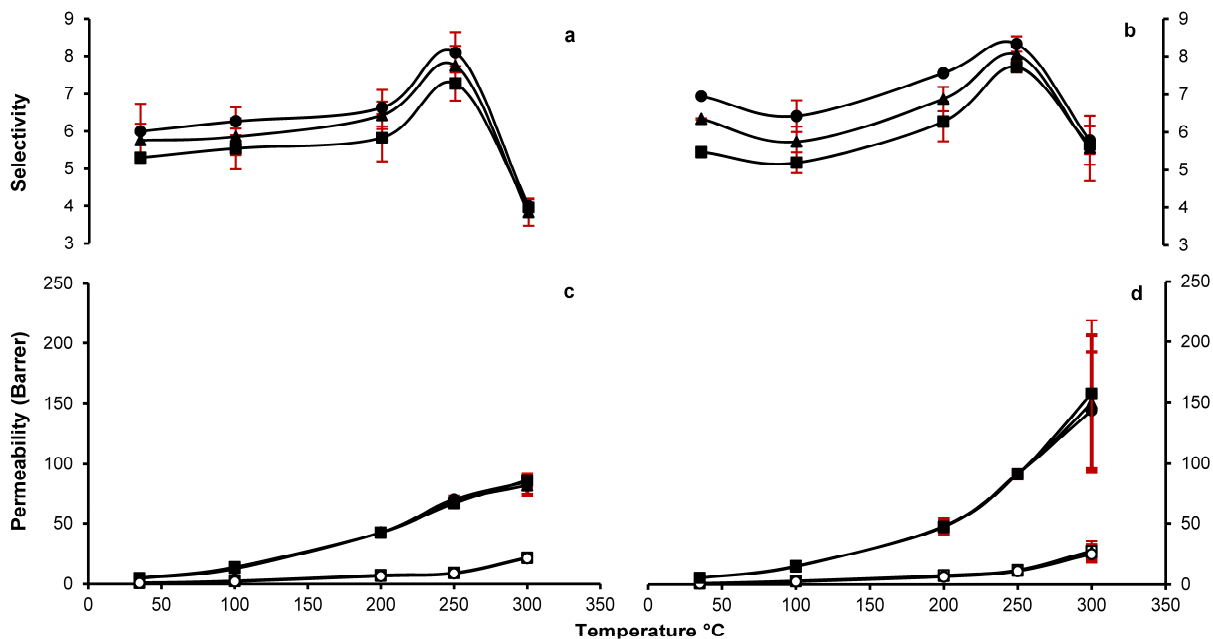


Figure 9. Ideal gas selectivity and permeability (H₂ solid, CO₂ open symbols) dependence on pressure and temperature for VTECTM (a, c) and for 20 wt% NH₂-MIL-53/VTECTM MMMs (b, d).

(■, □) = 5 bar, (▲, Δ) = 15 bar, (●, ○) = 30 bar.

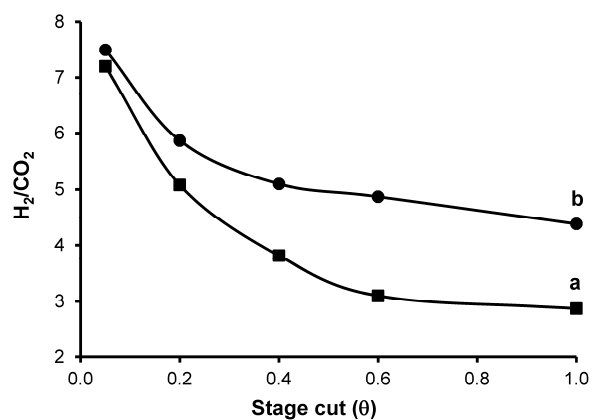


Figure 10. H₂/CO₂ selectivity from a 1:1 H₂/CO₂ mixture for a 20 wt% NH₂-MIL-53/VTECTM MMM (●) and a VTECTM (■) membrane. Membranes were tested at 30 bar and 250 °C.

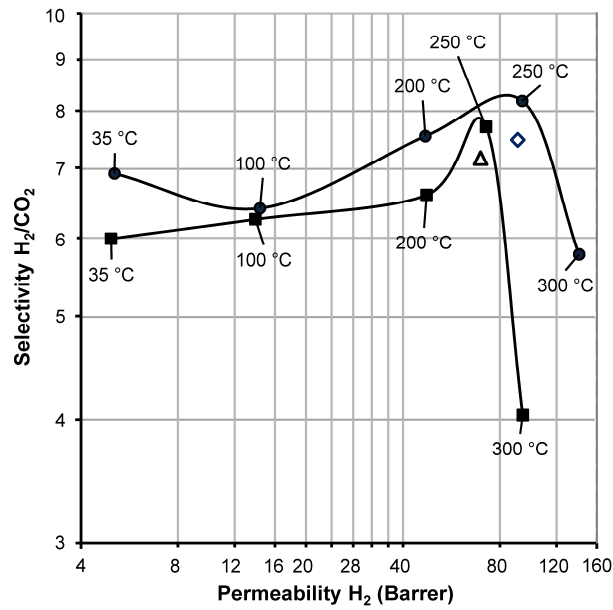


Figure 11. Log-log plot showing the performance of VTECTM and 20 wt% NH₂-MIL-53/VTECTM membranes at 30 bar and from 35 °C to 300 °C with pure gases (■ = VTECTM, ● = MMM) and with a 1:1 H₂/CO₂ mixture at $\theta = 0.05$ and 250 °C (Δ = VTECTM, \diamond = MMM).

Table 1. Pure gas permeability (Barrer) and ideal selectivity (average of 2 membranes) for VTECTM and 20 wt% NH₂-MIL-53/VTECTM MMMs from 35 °C to 300 °C at 5, 15, and 30 bar.

Temperature (°C)	Pressure (bar)	VTEC TM (Thicknesses: 10.2 and 12.6 μm)			20 wt% NH ₂ -MIL-53/VTEC TM (Thicknesses: 48.8 and 84.6 μm)		
		H ₂	CO ₂	H ₂ /CO ₂	H ₂	CO ₂	H ₂ /CO ₂
35	5	5.0 ± 0.7	1.0 ± 0.1	5.0 ± 0.1	5.4 ± 0.1	1.0 ± 0.1	5.4 ± 0.1
	15	4.7 ± 0.4	0.8 ± 0.1	5.8 ± 0.5	5.3 ± 0.2	0.8 ± 0.1	6.5 ± 0.1
	30	4.5 ± 0.3	0.7 ± 0.1	6.0 ± 0.7	5.1 ± 0.3	0.7 ± 0.1	7.0 ± 0.1
100	5	13.9 ± 0.3	2.5 ± 0.3	5.5 ± 0.5	15 ± 1	2.9 ± 0.1	5.2 ± 0.3
	15	13.3 ± 0.7	2.3 ± 0.3	5.8 ± 0.5	15 ± 1	2.6 ± 0.1	5.7 ± 0.4
	30	12.6 ± 0.4	2.0 ± 0.2	6.3 ± 0.4	15 ± 1	2.3 ± 0.1	6.5 ± 0.4
200	5	42.7 ± 0.2	7.4 ± 0.8	5.8 ± 0.6	47 ± 6	7.5 ± 0.4	6.3 ± 0.5
	15	42.8 ± 0.1	6.7 ± 0.4	6.4 ± 0.4	48 ± 5	7.0 ± 0.5	6.9 ± 0.3
	30	42.8 ± 0.6	6.5 ± 0.6	6.6 ± 0.5	48 ± 6	6.3 ± 0.8	7.6 ± 0.1
250	5	67 ± 3	9.2 ± 0.9	7.3 ± 0.5	91 ± 3	11.8 ± 0.6	7.7 ± 0.1
	15	69 ± 3	9.0 ± 0.9	7.7 ± 0.5	91 ± 3	11.3 ± 0.7	8.1 ± 0.2
	30	71 ± 3	8.7 ± 0.9	8.1 ± 0.5	91 ± 4	11.0 ± 0.7	8.3 ± 0.2
300	5	86 ± 6	21.7 ± 0.9	4.0 ± 0.1	157 ± 61	27 ± 8	5.7 ± 0.5
	15	82 ± 8	21.4 ± 0.1	3.8 ± 0.4	149 ± 56	26 ± 6	5.7 ± 0.9
	30	85 ± 4	21.2 ± 0.1	4.0 ± 0.2	144 ± 48	25 ± 7	5.8 ± 0.4

Table 2. H₂/CO₂ gas mixture separations of VTECTM and 20 wt% NH₂-MIL-53/VTECTM membranes with a 50/50 H₂/CO₂ feed at 250 °C and 30 bar at stage cuts from 0.05 to 1.

Stage cut (θ)	H ₂ /CO ₂ selectivity	
	VTEC TM (Thickness: 20.0 μm)	20 wt% NH ₂ -MIL-53/ VTEC TM (Thickness: 50.6 μm)
0.05	7.2	7.5
0.2	5.1	5.9
0.4	3.8	5.1
0.6	3.1	4.9
1.0	2.9	4.4

REFERENCES

- [1] Annual energy outlook 2014 early release overview, U.S. Energy Information Administration, 2014.
- [2] J. Conti, P. Holtberg, J.A. Beamon, S. Napolitano, A.M. Schaal, J.T. Turnure, L. Westfall, International energy outlook 2013, U.S. Energy Information Administration, DOE/EIA-0484, 2013.
- [3] A. Hellman, K. Honkala, S. Dahl, C.H. Christensen, J.K. Nørskov, Ammonia synthesis: State of the bellwether reaction, in J.R. Poeppelmeier (Ed.), *Comprehensive Inorganic Chemistry II*, Elsevier, Amsterdam, 2013, pp 459-474.
- [4] D.C.C. Habgood, A.F.A. Hoadley, L. Zhang, Techno-economic analysis of gasification routes for ammonia production from Victorian brown coal, *Chem. Eng. Res. Des.* 102 (2015) 57-68.
- [5] E. Shoko, B. McLellan, A.L. Dicks, J.C.D. da Costa, Hydrogen from coal: Production and utilisation technologies, *Int. J. Coal Geol.* 65 (3–4) (2006) 213-222.
- [6] G.Q. Lu, J.C. Diniz da Costa, M. Duke, S. Giessler, R. Socolow, R.H. Williams, T. Kreutz, Inorganic membranes for hydrogen production and purification: A critical review and perspective, *J. Colloid Interface Sci.* 314 (2) (2007) 589-603.
- [7] J.J. Marano, J.P. Ciferino, Integration of gas separation membranes with IGCC identifying the right membrane for the right job, in J. Yan (Ed.), *Energy Procedia* 1, Elsevier, 2009, pp 361-368.
- [8] K. Babita, S. Sridhar, K.V. Raghavan, Membrane reactors for fuel cell quality hydrogen through WGS – Review of their status, challenges and opportunities, *Int. J. Hydrogen Energy* 36 (11) (2011) 6671-6688.

- [9] F. Gallucci, E. Fernandez, P. Corengia, M. van Sint Annaland, Recent advances on membranes and membrane reactors for hydrogen production, *Chem. Eng. Sci.* 92 (2013) 40-66.
- [10] J.C. Diniz da Costa, G.P. Reed, K. Thambimuthu, High temperature gas separation membranes in coal gasification, *Energy Procedia* 1 (1) (2009) 295-302.
- [11] D.S. Newsome, The water-gas shift reaction, *Catal. Rev.* 21 (2) (1980) 275-318.
- [12] D. Driscoll, B. Morreale, L. Headley, NETL test protocol: Testing of hydrogen separation membranes, U.S. Department of Energy - National Energy Technology Laboratory, DOE/NETL-2008/1335, 2008.
- [13] M. Abdollahi, J. Yu, P.K.T. Liu, R. Ciora, M. Sahimi, T.T. Tsotsis, Hydrogen production from coal-derived syngas using a catalytic membrane reactor based process, *J. Membr. Sci.* 363 (1-2) (2010) 160-169.
- [14] D. Parsley, R.J. Ciora, Jr., D.L. Flowers, J. Laukaitaus, A. Chen, P.K.T. Liu, J. Yu, M. Sahimi, A. Bonsu, T.T. Tsotsis, Field evaluation of carbon molecular sieve membranes for the separation and purification of hydrogen from coal- and biomass-derived syngas, *J. Membr. Sci.* 450 (2014) 81-92.
- [15] G. Barbieri, A. Brunetti, G. Tricoli, E. Drioli, An innovative configuration of a Pd-based membrane reactor for the production of pure hydrogen: Experimental analysis of water gas shift, *J. Power Sources* 182 (1) (2008) 160-167.
- [16] A. Basile, A. Criscuoli, F. Santella, E. Drioli, Membrane reactor for water gas shift reaction, *Gas Separ. Purif.* 10 (4) (1996) 243-254.
- [17] A. Basile, E. Drioli, F. Santell, V. Violante, G. Capannelli, G. Vitulli, A study on catalytic membrane reactors for water gas shift reaction, *Gas Separ. Purif.* 10 (1) (1996) 53-61.

- [18] Y. Bi, H. Xu, W. Li, A. Goldbach, Water–gas shift reaction in a Pd membrane reactor over Pt/Ce_{0.6}Zr_{0.4}O₂ catalyst, *Int. J. Hydrogen Energy* 34 (7) (2009) 2965-2971.
- [19] O. Iyoha, R. Enick, R. Killmeyer, B. Howard, B. Morreale, M. Ciocco, Wall-catalyzed water-gas shift reaction in multi-tubular Pd and 80 wt%Pd–20 wt%Cu membrane reactors at 1173 K, *J. Membr. Sci.* 298 (1–2) (2007) 14-23.
- [20] S. Tosti, A. Basile, G. Chiappetta, C. Rizzello, V. Violante, Pd–Ag membrane reactors for water gas shift reaction, *Chem. Eng. J.* 93 (1) (2003) 23-30.
- [21] S. Battersby, S. Smart, B. Ladewig, S. Liu, M.C. Duke, V. Rudolph, J.C.D.d. Costa, Hydrothermal stability of cobalt silica membranes in a water gas shift membrane reactor, *Sep. Purif. Technol.* 66 (2) (2009) 299-305.
- [22] A. Brunetti, G. Barbieri, E. Drioli, T. Granato, K.H. Lee, A porous stainless steel supported silica membrane for WGS reaction in a catalytic membrane reactor, *Chem. Eng. Sci.* 62 (18–20) (2007) 5621-5626.
- [23] S.-J. Kim, Z. Xu, G.K. Reddy, P. Smirniotis, J. Dong, Effect of pressure on high-temperature water gas shift reaction in microporous zeolite membrane reactor, *Ind. Eng. Chem. Res.* 51 (3) (2011) 1364-1375.
- [24] G. Saracco, H.W.J.P. Neomagus, G.F. Versteeg, W.P.M.v. Swaij, High-temperature membrane reactors: potential and problems, *Chem. Eng. Sci.* 54 (13–14) (1999) 1997-2017.
- [25] L.Y. Jiang, T.S. Chung, Fabrication of mixed matrix hollow fibers with intimate polymer–zeolite interface for gas separation, *AIChE J.* 52 (8) (2006) 2898-2908.
- [26] L.Y. Jiang, T.S. Chung, R. Rajagopalan, Dual-layer hollow carbon fiber membranes for gas separation consisting of carbon and mixed matrix layers, *Carbon* 45 (2007) 166-172.

- [27] N. Peng, T.-S. Chung, J.-Y. Lai, The rheology of Torlon[®] solutions and its role in the formation of ultra-thin defect-free Torlon[®] hollow fiber membranes for gas separation, *J. Membr. Sci.* 326 (2) (2009) 608-617.
- [28] P. Bernardo, E. Drioli, G. Golemme, Membrane gas separation: A review/state of the art, *Ind. Eng. Chem. Res.* 48 (10) (2009) 4638-4663.
- [29] E.V. Perez, K.J. Balkus Jr, J.P. Ferraris, I.H. Musselman, Instrument for gas permeation measurements at high pressure and high temperature, *Rev. Sci. Instrum.* 84 (6) (2013) 065107-065107.
- [30] R.W. Baker, B.T. Low, Gas separation membrane materials: A perspective, *Macromolecules* 47 (20) (2014) 6999-7013.
- [31] E.V. Perez, K.J. Balkus Jr, J.P. Ferraris, I.H. Musselman, Mixed-matrix membranes containing MOF-5 for gas separations, *J. Membr. Sci.* 328 (1-2) (2009) 165-173.
- [32] T. Rodenas, M. van Dalen, E. Garcia-Perez, P. Serra-Crespo, B. Zornoza, F. Kapteijn, J. Gascon, Visualizing MOF mixed matrix membranes at the nanoscale: Towards structure-performance relationships in CO₂/CH₄ separation over NH₂-MIL-53(Al)@PI, *Adv. Funct. Mater.* 24 (2) (2014) 249-256.
- [33] H.B. Tanh Jeazet, C. Staudt, C. Janiak, Metal-organic frameworks in mixed-matrix membranes for gas separation, *Dalton Trans.* 41 (46) (2012) 14003-14027.
- [34] H. Ren, J. Jin, J. Hu, H. Liu, Affinity between metal-organic frameworks and polyimides in asymmetric mixed matrix membranes for gas separations, *Ind. Eng. Chem. Res.* 51 (30) (2012) 10156-10164.
- [35] T. Rodenas, M. van Dalen, P. Serra-Crespo, F. Kapteijn, J. Gascon, Mixed matrix membranes based on NH₂-functionalized MIL-type MOFs: Influence of structural and

operational parameters on the CO₂/CH₄ separation performance, *Micropor. Mesopor. Mater.* 192 (2014) 35-42.

[36] B. Seoane, J. Coronas, I. Gascon, M. Etxeberria Benavides, O. Karvan, J. Caro, F. Kapteijn, J. Gascon, Metal-organic framework based mixed matrix membranes: A solution for highly efficient CO₂ capture?, *Chem. Soc. Rev.* 44 (8) (2015) 2421-2454.

[37] B. Zornoza, C. Tellez, J. Coronas, J. Gascon, F. Kapteijn, Metal organic framework based mixed matrix membranes: An increasingly important field of research with a large application potential, *Micropor. Mesopor. Mater.* 166 (2013) 67-78.

[38] E. Perez, C. Karunaweera, I. Musselman, K. Balkus, J. Ferraris, Origins and evolution of inorganic-based and MOF-based mixed-matrix membranes for gas separations, *Processes* 4 (3) (2016) 32.

[39] E.V. Perez, K.J. Balkus Jr, J.P. Ferraris, I.H. Musselman, Metal-organic polyhedra 18 mixed-matrix membranes for gas separation, *J. Membr. Sci.* 463 (2014) 82-93.

[40] J. Ma, Y. Ying, Q. Yang, Y. Ban, H. Huang, X. Guo, Y. Xiao, D. Liu, Y. Li, W. Yang, C. Zhong, Mixed-matrix membranes containing functionalized porous metal-organic polyhedrons for the effective separation of CO₂-CH₄ mixture, *Chem. Commun.* 51 (20) (2015) 4249-4251.

[41] C. Zhao, N. Wang, L. Wang, H. Huang, R. Zhang, F. Yang, Y. Xie, S. Ji, J.R. Li, Hybrid membranes of metal-organic molecule nanocages for aromatic/aliphatic hydrocarbon separation by pervaporation, *Chem. Commun.* 50 (90) (2014) 13921-13923.

[42] S. Couck, E. Gobechiya, C.E.A. Kirschhock, P. Serra-Crespo, J. Juan-Alcaniz, A. Martinez Joaristi, E. Stavitski, J. Gascon, F. Kapteijn, G.V. Baron, J.F.M. Denayer, Adsorption and separation of light gases on an amino-functionalized metal-organic framework: An adsorption and in situ XRD study, *ChemSusChem* 5 (4) (2012) 740-750.

- [43] A. Boutin, S. Couck, F.-X. Coudert, P. Serra-Crespo, J. Gascon, F. Kapteijn, A.H. Fuchs, J.F.M. Denayer, Thermodynamic analysis of the breathing of amino-functionalized MIL-53(Al) upon CO₂ adsorption, *Micropor. Mesopor. Mater.* 140 (1-3) (2011) 108-113.
- [44] T. Ahnfeldt, D. Gunzelmann, T. Loiseau, D. Hirsemann, J. Senker, G. Ferey, N. Stock, Synthesis and modification of a functionalized 3D open-framework structure with MIL-53 topology, *Inorg. Chem.* 48 (7) (2009) 3057-3064.
- [45] Diamond V.4.0.4, Crystal Impact, Bonn, Germany, 2016.
- [46] F. Zhang, X. Zou, X. Gao, S. Fan, F. Sun, H. Ren, G. Zhu, Hydrogen selective NH₂-MIL-53(Al) MOF membranes with high permeability, *Adv. Funct. Mater.* 22 (17) (2012) 3583-3590.
- [47] B. Zornoza, A. Martinez-Joaristi, P. Serra-Crespo, C. Tellez, J. Coronas, J. Gascon, F. Kapteijn, Functionalized flexible MOFs as fillers in mixed matrix membranes for highly selective separation of CO₂ from CH₄ at elevated pressures, *Chem. Commun.* 47 (33) (2011) 9522-9524.
- [48] T. Lescouet, J.G. Vitillo, S. Bordiga, J. Canivet, D. Farrusseng, An alternative pathway for the synthesis of isocyanato- and urea-functionalised metal-organic frameworks, *Dalton Trans.* 42 (23) (2013) 8249-8258.
- [49] J. Gascon, U. Aktay, M.D. Hernandez-Alonso, G.P.M. van Klink, F. Kapteijn, Amino-based metal-organic frameworks as stable, highly active basic catalysts, *J. Catal.* 261 (1) (2009) 75-87.
- [50] J.R. Klaehn, C.J. Orme, E.S. Peterson, T.A. Luther, M.G. Jones, A.K. Wertsching, J.M.U. Klaehn, CO₂ separation using thermally optimized membranes: A comprehensive project report (2000-2007), Idaho National Laboratory, Idaho Falls, INL/EXT-07-12376, 2008.

- [51] C.J. Orme, J.R. Klaehn, F.F. Stewart, Membrane separation processes for the benefit of the sulfur–iodine and hybrid sulfur thermochemical cycles, *Int. J. Hydrogen Energy* 34 (9) (2009) 4088-4096.
- [52] S. Couck, T. Remy, G.V. Baron, J. Gascon, F. Kapteijn, J.F.M. Denayer, A pulse chromatographic study of the adsorption properties of the amino-MIL-53 (Al) metal-organic framework, *Phys. Chem. Chem. Phys.* 12 (32) (2010) 9413-9418.
- [53] J.O. Hsieh, K.J. Balkus Jr, J.P. Ferraris, I.H. Musselman, MIL-53 frameworks in mixed-matrix membranes, *Micropor. Mesopor. Mater.* 196 (2014) 165-174.
- [54] M. Karabacak, M. Cinar, Z. Unal, M. Kurt, FT-IR, UV spectroscopic and DFT quantum chemical study on the molecular conformation, vibrational and electronic transitions of 2-aminoterephthalic acid, *J. Mol. Struct.* 982 (1–3) (2010) 22-27.
- [55] R. Narayanan, R.M. Laine, Synthesis of soluble aluminium carboxylates directly from aluminium hydroxide, *J. Mater. Chem.* 10 (9) (2000) 2097-2104.
- [56] C.C. Landry, N. Pappé, M.R. Mason, A.W. Apblett, A.N. Tyler, A.N. MacInnes, A.R. Barron, From minerals to materials: Synthesis of alumoxanes from the reaction of boehmite with carboxylic acids, *J. Mater. Chem.* 5 (2) (1995) 331-341.
- [57] G.M. Shi, T. Yang, T.S. Chung, Polybenzimidazole (PBI)/zeolitic imidazolate frameworks (ZIF-8) mixed matrix membranes for pervaporation dehydration of alcohols, *J. Membr. Sci.* 415–416 (2012) 577-586.
- [58] J.A. Thompson, K.W. Chapman, W.J. Koros, C.W. Jones, S. Nair, Sonication-induced Ostwald ripening of ZIF-8 nanoparticles and formation of ZIF-8/polymer composite membranes, *Micropor. Mesopor. Mater.* 158 (2012) 292-299.

- [59] S. Diaham, M.L. Locatelli, T. Lebey, D. Malec, Thermal imidization optimization of polyimide thin films using Fourier transform infrared spectroscopy and electrical measurements, *Thin Solid Films* 519 (6) (2011) 1851-1856.
- [60] W.R. Vieth, K.J. Sladek, A model for diffusion in a glassy polymer, *J. Colloid Sci.* 20 (9) (1965) 1014-1033.
- [61] W.J. Koros, Model for sorption of mixed gases in glassy polymers, *J. Polymer Sci. Polymer Phys. Ed.* 18 (5) (1980) 981-992.
- [62] D.R. Paul, Gas sorption and transport in glassy polymers, *Ber. Bunsen-Ges. Phys. Chem.* 83 (1979) 294-302.
- [63] W.J. Koros, D.R. Paul, A.A. Rocha, Carbon dioxide sorption and transport in polycarbonate, *J. Polymer Sci. Polymer Phys. Ed.* 14 (4) (1976) 687-702.
- [64] W.J. Koros, D.R. Paul, Observations concerning the temperature dependence of the Langmuir sorption capacity of glassy polymers, *J. Polymer Sci. Polymer Phys. Ed.* 19 (10) (1981) 1655-1656.
- [65] T.T. Moore, W.J. Koros, Gas sorption in polymers, molecular sieves, and mixed matrix membranes, *J. Appl. Polym. Sci.* 104 (6) (2007) 4053-4059.
- [66] S. Couck, J.F.M. Denayer, G.V. Baron, T. Remy, J. Gascon, F. Kapteijn, An amine-functionalized MIL-53 metal-organic framework with large separation power for CO₂ and CH₄, *J. Am. Chem. Soc.* 131 (18) (2009) 6326-6327.
- [67] L.M. Robeson, The upper bound revisited, *J. Membr. Sci.* 320 (1-2) (2008) 390-400.
- [68] B.W. Rowe, L.M. Robeson, B.D. Freeman, D.R. Paul, Influence of temperature on the upper bound: Theoretical considerations and comparison with experimental results, *J. Membr. Sci.* 360 (1-2) (2010) 58-69.

- [69] B.W. Rowe, L.M. Robeson, B.D. Freeman, D.R. Paul, Corrigendum to “Influence of temperature on the upper bound: Theoretical considerations and comparison with experimental results” [J. Membr. Sci. 360 (2010) 58–69], J. Membr. Sci. 366 (1–2) (2011) 436.
- [70] D.R. Pesiri, B. Jorgensen, R.C. Dye, Thermal optimization of polybenzimidazole meniscus membranes for the separation of hydrogen, methane, and carbon dioxide, J. Membr. Sci. 218 (1–2) (2003) 11-18.
- [71] Q. Song, S.K. Nataraj, M.V. Roussenova, J.C. Tan, D.J. Hughes, W. Li, P. Bourgoin, M.A. Alam, A.K. Cheetham, S.A. Al-Muhtaseb, E. Sivaniah, Zeolitic imidazolate framework (ZIF-8) based polymer nanocomposite membranes for gas separation, Energy Environ. Sci. 5 (8) (2012) 8359-8369.
- [72] C.E. Powell, X.J. Duthie, S.E. Kentish, G.G. Qiao, G.W. Stevens, Reversible diamine cross-linking of polyimide membranes, J. Membr. Sci. 291 (1–2) (2007) 199-209.
- [73] L. Shao, T.-S. Chung, S.H. Goh, K.P. Pramoda, Polyimide modification by a linear aliphatic diamine to enhance transport performance and plasticization resistance, J. Membr. Sci. 256 (1–2) (2005) 46-56.
- [74] S. Japip, K.-S. Liao, Y. Xiao, T.-S. Chung, Enhancement of molecular-sieving properties by constructing surface nano-metric layer via vapor cross-linking, J. Membr. Sci. 497 (2016) 248-258.
- [75] N. Rangnekar, N. Mittal, B. Elyassi, J. Caro, M. Tsapatsis, Zeolite membranes - a review and comparison with MOFs, Chem. Soc. Rev. 44 (20) (2015) 7128-7154.
- [76] C. Güenther, H. Richter, I. Voigt, Zeolite membranes for hydrogen and water separation under harsh conditions, Chem. Eng. Trans. 32 (2013) 1963-1968.

[77] H. Li, K. Haas-Santo, U. Schygulla, R. Dittmeyer, Inorganic microporous membranes for H₂ and CO₂ separation—Review of experimental and modeling progress, *Chem. Eng. Sci.* 127 (2015) 401-417.

[78] J. Yao, H. Wang, Zeolitic imidazolate framework composite membranes and thin films: Synthesis and applications, *Chem. Soc. Rev.* 43 (13) (2014) 4470-4493.

